Dynamical screening in the scanning tunneling microscope and metal-insulator-metal junctions

Šestović, Dragan; Marušić, Leonardo; Šunjić, Marijan

Source / Izvornik: **Physical review B: Condensed matter and materials physics, 1997, 55, 1741 - 1747**

Journal article, Published version
Rad u časopisu, Objavljena verzija rada (izdavačev PDF)

Permanent link / Trajna poveznica: https://urn.nsk.hr/urn:nbn:hr:217:930128

Rights / Prava: In copyright / Zaštićeno autorskim pravom.

Download date / Datum preuzimanja: **2025-01-25**

Repository / Repozitorij:

Repository of the Faculty of Science - University of Zagreb

Dynamical screening in the scanning tunneling microscope and metal-insulator-metal junctions

D. Šestović,* L. Marušić, and M. Šunjić
Department of Physics, University of Zagreb, P.O.B. 162, 1000 Zagreb, Croatia
(Received 26 April 1996; revised manuscript received 26 August 1996)

We investigate electron tunneling in a system consisting of two curved metal surfaces separated by insulator or vacuum. In particular, we calculate the modifications of the tunneling barrier due to dynamical screening, i.e., interaction with charge fluctuations. We apply our general results to the planar metal-insulator-metal (MIM) junction, and to the scanning tunneling microscope (STM), describing the tip and the sample surface in STM by two rotational hyperboloids. We analyze the influence of the shape, dielectric properties, and work functions of both metals on the tunneling characteristics in the MIM and STM systems. For metals with different plasma frequencies, charge-fluctuation modes are effectively decoupled, and the electron interaction with these modes is significantly different than in the case of like metals, causing asymmetry in the barrier and also in the tunneling currents and conductivities. We also show that, for geometrical reasons, the tunneling barrier in the STM is lowered near the tip apex, which leads to focusing of the tunneling current and increased lateral resolution of STM. [S0163-1829(96)06148-6]

I. INTRODUCTION

Common applications of electron tunneling in the solid state physics are metal-insulator-metal junction (MIM),[1] scanning tunneling microscopy (STM),[2] and other similar techniques such as, e.g., ballistic electron emission microscopy (BEEM).[3] By MIM we mean a system consisting of two metal electrodes with planar surfaces, separated by a thin insulator (or vacuum) layer, or any system with equivalent electrical properties, such as a semiconductor heterojunction (e.g., Esaki's diode[1]). STM can be considered theoretically as a complicated example of MIM, where the surfaces are not at all planar and they are of different materials. These systems are becoming increasingly interesting due, e.g., to the development of crystal growth techniques, and for all of them we need a successful description of an effective potential barrier affecting the tunneling electron. This is especially important in STM where, so far, there is no theory that sufficiently well explains the high resolution obtained in the STM images.

There are many studies of the electron tunneling between the curved metallic surfaces as in STM (Refs. 4–11) or in the similar problem of TPFG (textured polysilicon floating gate) EEPROM (electrically erasable programmable read-only memory).[12] Their authors developed interesting methods for solving the problem of electron tunneling in such cases, but they used barriers that are either simple rectangular, or parametrized classical barriers,[13,14] without any microscopic detail, or at most barriers calculated within the framework of the density functional theory in the local density approximation (LDA).[15,16]

Calculation of the tunneling barrier for a realistic physical problem is still a formidable task, and *ab initio* calculations of the image potential, that would take into account both the band structure of the metal and the dynamical effects, do not exist even for the simplest geometry. Most accurate image potentials are probably obtained for the semi-infinite jellium surface via diagrammatic corrections of the LDA results.[17,18] Although these results are based on a very detailed description of the response that contains a complete spectrum of excitations in a solid, they are not quite appropriate for studying STM, because they describe interaction of an electron with a flat surface and do not take into account coupling of the charge fluctuations on curved and different surfaces (which is strong because the surfaces are very close).

In the MIM system, it is easier to study charge-fluctuation modes, due to translational invariance in the direction parallel to the surface. Several studies of the response[19–24] took into account only surface plasmons (SP), neglecting bulk modes and single particle excitations. The situation is much more complex in the case of STM, where a three-dimensional (3D) problem could not be reduced to a one-dimensional (problem). It is practically impossible to perform a nonlocal quantum mechanical calculation, but even a local limit[24,20] was never obtained.

In this paper we want therefore to take into account coupling of charge-fluctuation modes on two curved surfaces, and calculate the resulting dynamical potential affecting the tunneling electron. In order to emphasize the influence of the curved geometry and coupling of two surfaces, we start with the potential barrier of simple rectangular shape (Sommerfeld model) and metal surfaces with different work functions, and study the modification of this barrier due to charge-fluctuation modes.

We investigate a general system consisting of two different, possibly curved metal surfaces. Therefore we need a 3D calculation, and we adopt a local, but also a semiclassical limit, treating the electron as a classical point charge.[25,26] We describe charge fluctuations in both metals using a long-wavelength limit, coupling the tunneling electron to surface plasmons only.[27] We calculate dispersion relations of the coupled SP modes, their interaction with the classical electron, the total potential barrier, the tunneling currents, and conductivities.

 © 1997 The American Physical Society

Because the theory is general and independent of the particular shape of surfaces (assuming only that surfaces can be described in the coordinate system in which the Laplace equation is separable), we shall first calculate the modes, their dispersion relations, and interaction in general coordinates, and then apply these results to some particular cases.

The first obvious application is the MIM junction in a planar geometry, where the problem can be solved in Cartesian coordinates. If our electrodes are made of different metals, i.e., have appreciably different bulk plasma frequencies (ω_p), we find that SP's on two surfaces are effectively decoupled, which leads to an overall reduction of the tunneling barrier. This difference in the ω_p's causes asymmetries in the tunneling barriers. By calculating the tunneling current we demonstrate that the finite contact potential is not the only source of the asymmetries in the I-V curves and offset in the conductivity minimum.

In the STM case the tip is represented by the rotational hyperboloid,[28] and the sample surface could be either flat or slightly curved upwards or downwards (also in the shape of a rotational hyperboloid), in order to simulate protrusions or deflections on the sample surface. This model only roughly resembles the real shape of the system, and does not take into account any atomic protrusion on the tip, but its important advantage is that dynamical screening for both surfaces can be described in a closed form. Chemical composition of the tip due to absorbed nonmetallic atoms at the tip apex also has not been taken into account, but a recent study[29] shows that there is no obvious correlation between the effective barrier height and the kind of chemical species at the tip apex. These authors conclude that the influence of the tip shape, i.e., the tip radius is more important, in agreement with our results. As shown in a preliminary paper, Ref. 30, the potential barrier is found to be lowered near the symmetry axis. We show here, using quasiclassical approximation, that such a change of a potential leads to the focusing of the tunneling electrons and increased lateral sensitivity of STM. Different curvatures of the tip and sample are additional sources of asymmetries in the tunneling barriers causing asymmetrical I-V curves[30] as has been already observed experimentally.[31] Asymmetry in tunneling is also shown as offset in the conductivity minimum similar to those caused by the finite contact potential.[32]

II. FORMULATION OF THE PROBLEM

We describe interaction of the tunneling electron with the SP in the local semiclassical approximation, since full nonlocal quantum mechanical treatment is, so far, possible only for a single planar surface. As we are mainly interested in the situation when the electron is in the barrier region, we neglect bulk plasmons and electron-hole pairs, reducing charge fluctuations in a metal to surface plasmons. These approximations are certainly not valid for the electron in the metal and very close to the surface, but they are necessary due to the complicated geometry of our system. Therefore our Hamiltonian is[27]

$$H=\frac{\mathbf{p}_e^2}{2m}+U(\mathbf{r})+\sum_q \hbar\omega_q\left(b_q^\dagger b_q+\frac{1}{2}\right)+\sum_q [\Gamma_q(\mathbf{r})b_q^\dagger+\text{H.c.}]. \tag{1}$$

The first two terms are electron kinetic and potential energies, respectively, the third term describes SP oscillations, and q is a set of quantum numbers for a specific symmetry. The fourth term represents the interaction, and Γ's are matrix elements of the electron-SP interaction.[21,26,27,33]

The one-electron potential is given by

$$U(\mathbf{r})=V_{\text{FBM}}(\mathbf{r})+V_{\text{el}}(\mathbf{r}). \tag{2}$$

V_{FBM} is a standard rectangular potential barrier [finite barrier model (FBM)], with contributions from interaction with the ions and electrons in a metal (i.e., band structure effects). $V_{\text{el}}(\mathbf{r})$ is part of the electrostatic potential due to different work functions of the metals and the external voltage.

Hamiltonian (1) can be easily diagonalized,[34] leading to the effective barrier for an electron at point $\mathbf{r}$:

$$V(\mathbf{r})=U(\mathbf{r})-\sum_q \frac{|\Gamma_q(\mathbf{r})|^2}{\hbar\omega_q}, \tag{3}$$

where the second term represents the energy shift or the image potential. This term will be calculated only in the tunneling or vacuum (insulator) region, keeping in mind that our approximation is not valid in the metal region. For SP's in the long-wavelength approximation, we have to introduce quantum corrections by summing up to a cutoff wave vector q_c which is related to the Landau damping of collective plasmon modes into electron-hole pairs.

III. SURFACE PLASMON MODES

We calculate SP modes and their dispersion for a system consisting of two curved metal surfaces (denoted by subscripts 1 and 2) separated by vacuum (denoted by 0). We restrict ourselves to surfaces coinciding with the coordinate surfaces of orthogonal coordinate systems in which the Laplace equation is separable.[28] Therefore we introduce the generalized coordinates u_1,u_2,u_3 where the coordinate u_1 is perpendicular to both surfaces, and the other two are parallel to them. Metal surfaces are defined by $u_1=u_1^1$ and $u_1=u_1^2$.

Surface polarization modes are solutions of the Laplace equation:[25]

$$\triangle\Phi=0. \tag{4}$$

If we separate (4), and denote by $A_q(u_2,u_3)$ the solution in the direction parallel to the surfaces, and by $B_{1q}(u_1)$ and $B_{2q}(u_1)$ solutions in the direction perpendicular to the surfaces and regular in the regions 1 and 2, respectively, we can write a general solution as

$$\Phi_q(\mathbf{r})=\begin{cases} C_1B_{1q}(u_1)A_q(u_2,u_3) & \text{in metal 1} \\ [C_3B_{1q}(u_1)+C_4B_{2q}(u_1)]A_q(u_2,u_3) & \text{in vacuum} \\ C_2B_{2q}(u_1)A_q(u_2,u_3) & \text{in metal 2.} \end{cases} \tag{5}$$

We apply standard boundary conditions for the fields $\mathbf{E}=-\nabla\Phi$ and $\mathbf{D}=\epsilon\mathbf{E}$ on both surfaces:

$$(E_{\text{in}})_t=(E_{\text{out}})_t, \quad (D_{\text{in}})_n=(D_{\text{out}})_n. \tag{6}$$

Metal dielectric functions in the long-wavelength limit are

$$\epsilon_{1,2}=1-\frac{\omega_{p1,2}^2}{\omega^2}, \tag{7}$$

and we assume that in the barrier region $\epsilon=1$.

Using (5) and (6) we get the relation between the dielectric function and the wave vector, which using (7) leads to the dispersion relation $\omega(q)$ of the SP. If we choose $C_1=1$, the other coefficients are given by

$$C_2=C_3\frac{B_{12}}{B_{22}}+C_4, \tag{8a}$$

$$C_3=1-\frac{(\epsilon_1-1)B_{21}B_{11}'}{W}, \tag{8b}$$

$$C_4=\frac{(\epsilon_1-1)B_{11}B_{11}'}{W}, \tag{8c}$$

where B_{ij} denotes the value of the function B_{ik} at the surface u_1^j, a prime denotes derivative with respect to u_1, and W is the Wronskian:

$$W=B_{11}B_{21}'-B_{21}B_{11}'. \tag{9}$$

The analytical expression for the dispersion relation is rather lengthy, so we shall not write it in the general form, but rather discuss it for specific geometries.

IV. COUPLING MATRIX ELEMENTS

The matrix element of the interaction of an electron at $\mathbf{r}$ with charge e with the surface polarization modes is given by[26]

$$\Gamma_q(\mathbf{r})=\sum_i \sqrt{\frac{\hbar e^2\omega_{pi}^2}{8\pi\omega_q S}}\int_{S_i}\frac{\mathbf{P}_q(\mathbf{r}_i)}{|\mathbf{r}-\mathbf{r}_i|}dS_i, \tag{10}$$

where index i denotes the metal electrode (1 or 2), and $\mathbf{P}_q$ are surface polarization eigenmodes, given by

$$\mathbf{P}_q(\mathbf{r})=\omega_p^2\frac{\nabla\Phi_q(\mathbf{r})}{\sqrt{N_q}}. \tag{11}$$

N_q is the normalization constant determined by

$$\int_V \mathbf{P}_q\mathbf{P}_{q'}dV=\delta(q-q'). \tag{12}$$

We can expand $1/|\mathbf{r}-\mathbf{r}'|$ in terms of solutions of the Laplace equation:[35]

$$\frac{1}{|\mathbf{r}-\mathbf{r}'|}=-4\pi\sqrt{\frac{g_{11}'}{g_{22}'g_{33}'}}\sum\frac{\rho(u_2,u_3)}{M_q}A_q^*(u_2',u_3') \times A_q(u_2,u_3)\frac{1}{W}\begin{cases} B_{1q}(u_1)B_{2q}(u_1') & \text{if } u_1>u_1' \\ B_{2q}(u_1)B_{1q}(u_1') & \text{if } u_1<u_1', \end{cases} \tag{13}$$

where g_{ii} are the metric coefficients of the generalized coordinate system,

$$g_{ii}=\left(\frac{\partial x}{\partial u^i}\right)^2+\left(\frac{\partial y}{\partial u^i}\right)^2+\left(\frac{\partial z}{\partial u^i}\right)^2, \tag{14}$$

while $\rho(u_2,u_3)$ and M_q are determined from the condition

$$\int\int d(u_2)d(u_3)A_q^*(u_2,u_3)A_{q'}(u_2,u_3)\rho(u_2,u_3) =M_q\delta_{q,q'}. \tag{15}$$

Using relations (10)–(15) we can get the coupling matrix elements (per surface area S) as will be shown later for some specific cases.

V. APPLICATION TO THE PLANAR MIM JUNCTIONS

We can easily apply these general results to the case of electron tunneling between planar metal surfaces as in MIM junctions. We use Cartesian coordinate system $\mathbf{r}\equiv(\boldsymbol{\rho},z)$, with the z axis perpendicular to the metal surfaces determined by z_1 and z_2, and q is a wave vector $\mathbf{k}$ parallel to the surface.

Solutions of the Laplace equation are

$$A_k(\boldsymbol{\rho})=e^{i\mathbf{k}\cdot\boldsymbol{\rho}}, \quad B_{p,k}=e^{\pm kz}. \tag{16}$$

This leads to the dispersion relation

$$\omega_k=\frac{\omega_{p1}}{2}\sqrt{1+r^2\pm\sqrt{1+r^4-r^2(2-4e^{2k(z_1-z_2)})}}, \tag{17}$$

where

$$r=\frac{\omega_{p2}}{\omega_{p1}}. \tag{18}$$

The coupling matrix elements (in the barrier region) are

$$\Gamma_k(\mathbf{r})=-\sqrt{\frac{\pi\hbar e^2}{2\omega_k}}\frac{1}{\sqrt{N_k}} \times(C_1\omega_{p1}^3e^{2kz_1-kz}+C_2\omega_{p2}^3e^{-2kz_2+kz}), \tag{19}$$

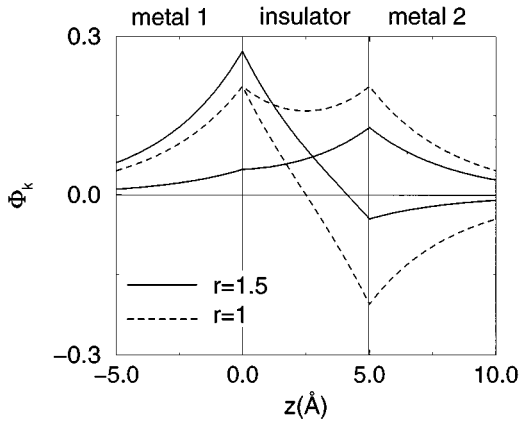

FIG. 1. SP modes in the planar MIM case. Dashed curves represent the case $r=\omega_{p2}/\omega_{p1}=1$ and solid curves represent the case $r=1.5$.

where

$$N_k=4\pi^2k(C_1^2\omega_{p1}^4e^{2kz_1}+C_2^2\omega_{p2}^4e^{-2kz_2}). \tag{20}$$

SP modes are shown in Fig. 1. One mode oscillates in phase (IP mode) on both surfaces, and the second oscillates out of phase (OP mode). For $r=1$ IP modes are symmetrical and OP modes are antisymmetrical, but for $r\neq1$ this symmetry is broken. In that case IP/OP modes are located mainly at the surface of metal with larger/smaller ω_p, and their frequencies approach asymptotically SP frequencies of these metals ($\omega_{s,i}=\omega_{p,i}/\sqrt{2}$), causing a gap in the dispersion relation, as shown in Fig. 2, where the upper curves represent IP modes and the lower represent OP modes.

The total tunneling barrier can be obtained from (3). We can see in Fig. 3 how effective decoupling of SP for $r\neq1$ leads to the reduction and asymmetries in effective tunneling barriers. Total reduction of the barrier is caused by the fact that the electron weakly interacts with the antisymmetrical mode. Therefore for $r=1$ the main contribution comes from interaction with the IP mode, while the interaction with the OP mode is almost negligible. On the other hand, for $r\neq1$ interaction with both modes is stronger, so the total effect is larger than in the $r=1$ case. Obviously the interaction with

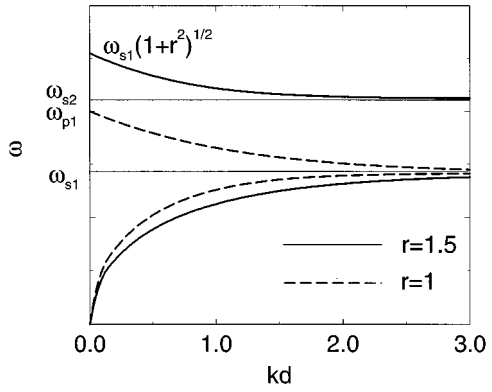

FIG. 2. SP dispersion curves in the planar MIM case. As in Fig. 1 dashed curves represent the case $r=\omega_{p2}/\omega_{p1}=1$ and solid curves represent the case $r=1.5$.

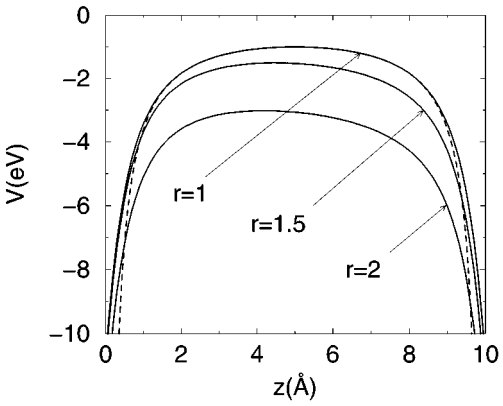

FIG. 3. Tunneling barriers in planar MIM case for the cases $r=1$, $r=1.5$, $r=2$, where distance between the metal surfaces is $d=10$ Å. The dashed line represents the classical image potential.

IP modes dominates, so the lowering of the barrier is bigger near the surface at which the coupling to the IP mode is located, causing asymmetries in effective tunneling barriers. Asymmetries in current-voltage curves seen in planar metal-insulator-metal junctions[32] are caused partly by this effect and partly by the contact potential due to different work functions. In order to demonstrate it we calculated the tunneling current density by Straton's formula,[36] where the tunneling probability was given in the WKB approximation:

$$j(V)=\frac{4\pi m_e\exp(-b_1)}{h^3c_1^2}[1-\exp(-c_1V)], \tag{21}$$

where

$$b_1(V)=\sqrt{\frac{8m}{\hbar^2}}\int_{z_{1t}}^{z_{2t}}\sqrt{V(z)-E_F}\,dz, \tag{22}$$

$$c_1(V)=\sqrt{\frac{2m}{\hbar^2}}\int_{z_{1t}}^{z_{2t}}\frac{1}{\sqrt{V(z)-E_F}}\,dz. \tag{23}$$

Results are shown in Fig. 4, where we can see that for increasing r, the I-V curve is more asymmetrical and the

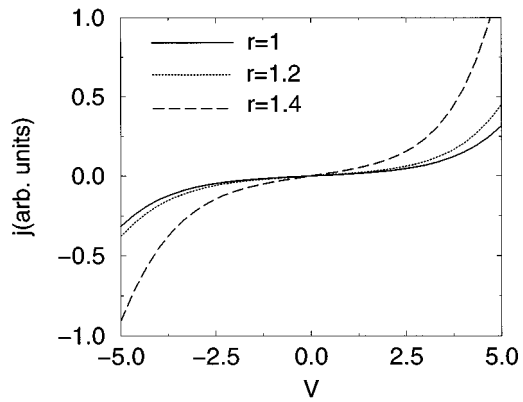

FIG. 4. I-V curves for the cases $r=1$, $r=1.2$, $r=1.4$, where the distance between the metal surfaces is $d=5$ Å.

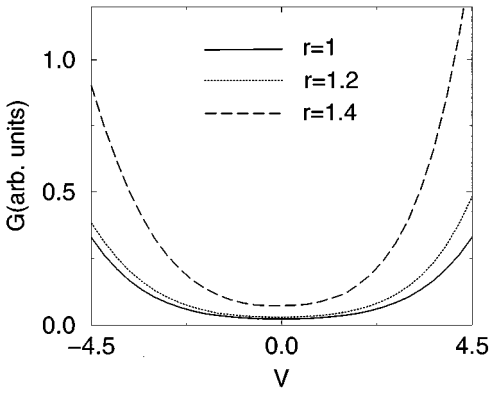

FIG. 5. Tunneling conductivity for the cases $r=1$, $r=1.2$, $r=1.4$, and for the distance $d=5$ Å.

currents are larger. Asymmetries in tunneling are also shown in Fig. 5 where we present the calculated conductivity $G=\partial j/\partial V$.

It is important to emphasize that generally there is no obvious correlation between the work function and SP frequency, i.e., the sign of the contact potential is not directly related to the ratio of SP frequencies. Therefore asymmetries due to these origins could sometimes add, but sometimes could also cancel.

VI. APPLICATION TO THE STM

In the STM the system consists of two curved surfaces of different metals. We describe them by two rotational hyperboloids — one very narrow (tip), and the other much wider (sample). The sample surface could be curved upwards or downwards (simulating deflection or protrusion, respectively), or just flat. For simplicity the center of this deflection (protrusion) will be placed directly below the center of the tip, so that their surfaces coincide with coordinate surfaces of the prolate spheroidal system.[28] Coordinates of this system are ξ, η, and φ, where φ is polar coordinate, ξ defines surfaces in the shape of confocal ellipsoids, and η defines surfaces in the shape of rotational hyperboloids ($\eta=\eta_1$ and $\eta=\eta_2$). The associated quantum numbers are the continuous ''wave vector'' κ and discrete angular quantum number m.

Since tunneling probability decays exponentially with distance, only the region near the tip apex is interesting, so important parameters of our problem are the curvatures of the tip $(1/R_1)$ and the sample $(1/R_2)$ at the z axis, and the distance (d) between the tip and the sample. They are related to the spheroidal coordinates by

$$R_{1,2}=a\frac{1-\eta_{1,2}^2}{\eta_{1,2}} \tag{24a}$$

and

$$d=a(\eta_1-\eta_2), \tag{24b}$$

where a is the focal length of ellipsoids and hyperboloids.

The Laplace equation in the spheroidal coordinate system is

$$\frac{1}{a^2(\xi^2-\eta^2)}\left\{\frac{\partial}{\partial\xi}\left[(\xi^2-1)\frac{\partial\Phi}{\partial\xi}\right]+\frac{\partial}{\partial\eta}\left[(1-\eta^2)\frac{\partial\Phi}{\partial\eta}\right]\right\}$$
$$+\cdots+\frac{1}{a^2(\xi^2-1)(1-\eta^2)}\frac{\partial\Phi^2}{\partial\varphi^2}=0, \tag{25}$$

and the general solutions are

$$\Phi_{\kappa,m}(\eta,\xi,\varphi)\propto P^m_{-1/2+i\kappa}(\pm\eta)P^m_{-1/2+i\kappa}(\xi)e^{im\varphi}, \tag{26}$$

where the plus sign refers to the solution in the tip and the minus sign to the solution in the sample, and $P^m_{-1/2+i\kappa}(x)$ is the conical function of the first kind.[37]

Electrostatic potential due to an applied external voltage $V_{\rm el}(\mathbf{r})$ can also be calculated by solving the Laplace equation with homogeneous boundary conditions, which leads to

$$V_{\rm el}(\eta)=V_0\frac{\ln\left\{\dfrac{[(1+\eta_2)(1-\eta)]}{[(1-\eta_2)(1+\eta)]}\right\}}{\ln\left\{\dfrac{[(1+\eta_2)(1-\eta_1)]}{[(1-\eta_2)(1+\eta_1)]}\right\}}. \tag{27}$$

Interaction matrix elements could be evaluated using the method shown in Sec. IV and in the vacuum they are

$$\Gamma_{\kappa,m}(\mathbf{r})=-\sqrt{\frac{2\pi\hbar e^2}{S\omega_{\kappa,m}N_{\kappa,m}}}P^m_{-1/2+i\kappa}(\xi)e^{im\varphi}$$
$$\times[\omega_{p1}^3\alpha_{m,\kappa}(\eta_1,\eta_2)P^m_{-1/2+i\kappa}(-\eta)$$
$$-\cdots-\omega_{p2}^3\beta_{m,\kappa}(\eta_1,\eta_2)P^m_{-1/2+i\kappa}(\eta)], \tag{28}$$

where

$$N_{\kappa,m}=\frac{2\pi^2\gamma_{m,\kappa}(\eta_1,\eta_2)}{\kappa sh(\pi\kappa)\Gamma(1/2-m+i\kappa)\Gamma(1/2-m-i\kappa)}, \tag{29}$$

$$\gamma_{m,\kappa}(\eta_1,\eta_2)=-aC_1^2(1-\eta_1^2)$$
$$\times[P^m_{-1/2+i\kappa}(\eta_1)]^*\left.\frac{\partial P^m_{-1/2+i\kappa}(\eta)}{\partial\eta}\right|_{\eta=\eta_1}$$
$$+aC_2{}^2(1-\eta_2^2)[P^m_{-1/2+i\kappa}(-\eta_2)]^*$$
$$\times\left.\frac{\partial P^m_{-1/2+i\kappa}(-\eta)}{\partial\eta}\right|_{\eta=\eta_2}, \tag{30}$$

$$\alpha_{m,\kappa}(\eta_1,\eta_2)=\frac{C_1}{W(\eta_1)}P^m_{-1/2+i\kappa}(\eta_1)\left.\frac{\partial P^m_{-1/2+i\kappa}(\eta)}{\partial\eta}\right|_{\eta=\eta_1}, \tag{31}$$

$$\beta_{m,\kappa}(\eta_1,\eta_2)=\frac{C_2}{W(\eta_2)}P^m_{-1/2+i\kappa}(-\eta_2)$$
$$\times\left.\frac{\partial P^m_{-1/2+i\kappa}(-\eta)}{\partial\eta}\right|_{\eta=\eta_2}, \tag{32}$$

and $W(\eta_i)$ are the Wronskians (9).

Dispersion relations of SP are shown in Ref. 30, where we can see the IP and OP modes, as in the planar case. Different curvatures and different ω_p's break their symmetry as shown

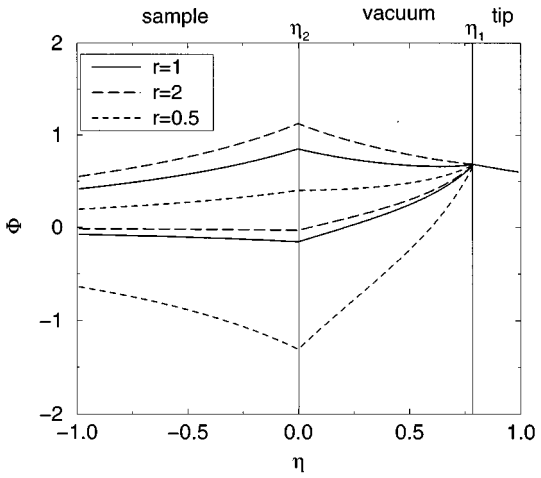

FIG. 6. SP modes in the STM case along the η coordinate, for different κ and ω_p. The tip surface is determined by η_1 and the sample by η_2.

in Fig. 6. In the case $r=1$ coupling to IP modes dominates near the electrode with smaller curvature (sample) and coupling to OP modes at the other side (tip).

Using relations (3) we calculate the total 3D tunneling barriers in the vacuum region for several specific geometries as shown in Fig. 7. This demonstrates that the effective tunneling barrier is significantly lowered in the region close to the tip apex, especially for smaller distances, which should be an additional source of focusing of the tunneling electrons.

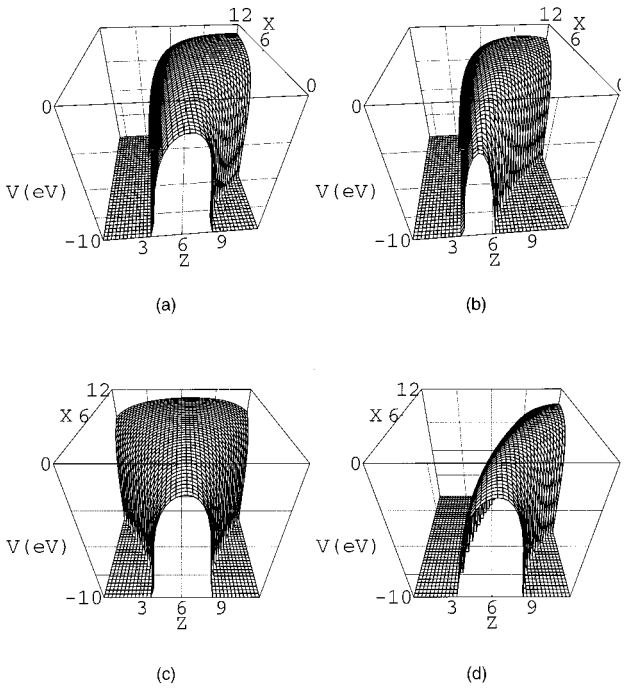

FIG. 7. Three-dimensional tunneling barriers in the x-z plane calculated for the case of the tungsten tip ($\omega_{p1}=9.9$ eV) with radius $R_1=3$ Å, above the aluminum sample ($\omega_1=15.3$ eV). The tip is above a flat sample in (a) where distance is $d=5$ Å and in (b) where distance is $d=3$ Å. The tip is above a protrusion in (c) where $d=5$ Å and sample radius of curvature is $R_2=3$ Å, and above a depression in (d) where $R_2=-10$ Å and distance is the same.

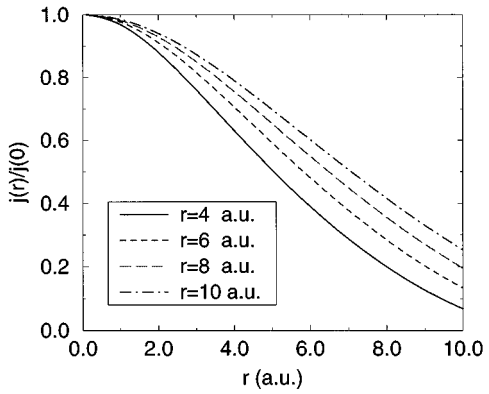

FIG. 8. Lateral distribution of the current density for different curvatures at the tip apex. Distance between the tip and the sample is $d=5$ a.u. and plasmon frequencies are the same as in Fig. 7.

In order to investigate focussing effect, we calculate the lateral distribution of the tunneling current on the sample surface. We use the quasiclassical approximation of the Schrödinger equation, applied to the problem of tunneling through the potential barrier, the equipotential surfaces of which coincide with η coordinate surfaces of the prolate spheroidal coordinate system. Tunneling distribution on surface η_2 is given by[12]

$$j(\xi,\eta,\varphi)=K_0\frac{H(\xi,\eta_1,\varphi)}{H(\xi,\eta_2,\varphi)} \times\exp\left(\frac{\sqrt{8m}}{\hbar}\int_{\eta_2}^{\eta_1}\sqrt{|E-V(\xi,\eta',\varphi)|}\right)h_\eta d\eta', \tag{33}$$

where

$$H(\xi,\eta,\varphi)=h_\xi(\xi,\eta,\varphi)h_\varphi(\xi,\eta,\varphi), \tag{34}$$

and h_ξ, h_η, and h_φ are metric coefficients of the prolate spheroidal coordinate system. K_0 is constant with the dimension of the electric current density.[12] In Fig. 8 we show the current density on the flat sample surface calculated as a function of radial distance. It is obvious that such focusing improves lateral resolution in the STM.

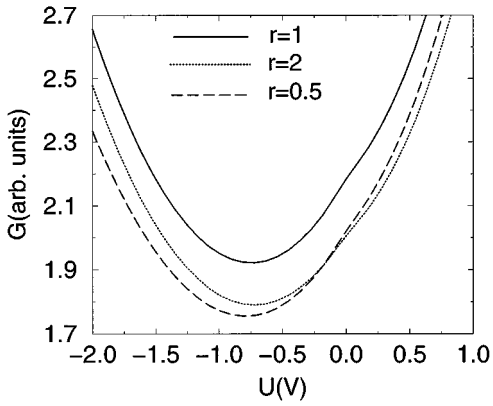

FIG. 9. Conductivities in the STM for the distance of the tip above the sample $d=5$ Å.

As was already shown,[31,30] electron tunneling is easier from the tip to the sample than in the opposite direction; this effect is caused by the different curvatures of the tip and the sample. Shapes of the tunneling characteristics, e.g., *I-V* curves or conductivities, depend on the curvatures of the electrodes, ω_p's, and the contact potential as shown in Fig. 5 of Ref. 30. Similar conclusions follow from the calculation of conductivity as shown in Fig. 9. We can see that the minimum of the paraboloidal-like curves shifts away from the zero bias similarly to the effect caused by the finite contact potential.[32]

VII. CONCLUSION

We have calculated the image potential reduction of the barrier due to the interaction of the tunneling electron with charge fluctuations — surface plasmons in a general system consisting of two metal surfaces separated by vacuum or insulator. The results can be used to study systems with the curved surfaces and here we have applied them to the planar MIM junctions and STM. The calculation of the total tunneling barrier enables us to analyze how it is influenced by geometrical parameters (curvatures of metal electrodes and their distance) and other parameters such as different bulk plasma frequencies (ω_p) and contact potential due to different work functions. We have explained the physical origin of the reduction of the tunneling barrier when the parameters of electrodes (ω_p's, curvatures) are different, caused by effective decoupling of SP's. These differences also cause asymmetry in the tunneling barrier, *I-V* curves, and conductivities, i.e., (i) tunneling is easier from the electrode with smaller ω_p to the electrode with larger ω_p; (ii) tunneling is easier from the electrode with smaller radius of curvature (tip) to the electrode with the larger radius of curvature (sample). We also found the offset in the conductivity minimum, caused by the differences in these parameters, similarly to the offset which was usually attributed only to the finite contact potential.[32] Also, we showed that the 3D tunneling barrier in STM is lowered near the tip apex which leads to focusing of electrons and to improvement of the lateral resolution in the STM images.

*Present address: Departamento de Física Teórica de la Materia Condensada, C-V. Universidad Autónoma, E-28049 Madrid, Spain.

[1] L. Esaki, J. Phys. (Paris) **45**, 3 (1984).
[2] G. Binnig and H. Rohrer, Rev. Mod. Phys. **59**, 615 (1987).
[3] M. Prietch, Phys. Rep. **253**, 163 (1995).
[4] N. Garcia, C. Ocal, and F. Flores, Phys. Rev. Lett. **50**, 2002 (1983).
[5] J. Tersoff and D. R. Hamann, Phys. Rev. B **31**, 805 (1985).
[6] N. D. Lang, Phys. Rev. Lett. **55**, 230 (1985).
[7] N. D. Lang, Phys. Rev. Lett. **56**, 1164 (1986).
[8] Balaram Das and J. Mahanty, Phys. Rev. B **36**, 898 (1987).
[9] A. A. Lucas, H. Morawitz, G. R. Henry, J. P. Vigneron, Ph. Lambin, P. H. Cutler, and T. E. Feuchtwang, Phys. Rev. B **37**, 10 708 (1988).
[10] Th. Laloyaux, I. Derycke, J.-P. Vigneron, Ph. Lambin, and A. A. Lucas, Phys. Rev. B **47**, 7508 (1993).
[11] D. Šestović and M. Šunjić, Phys. Rev. B **51**, 13 760 (1995).
[12] D. Rinaldi, S. Santini, and M. Vanzi, Semicond. Sci. Technol. **9**, 1414 (1994).
[13] G. Binnig, N. Garcia, H. Rohrer, J. M. Soler, and F. Flores, Phys. Rev. B **30**, 4816 (1984).
[14] J. M. Pitarke, P. M. Echenique, and F. Flores, Surf. Sci. **217**, 267 (1989).
[15] N. D. Lang and W. Kohn, Phys. Rev. B **7**, 3541 (1973).
[16] N. D. Lang, Phys. Rev. B **37**, 10 395 (1988).
[17] A. G. Eguiluz, M. Heinrichsmeier, A. Fletzar, and W. Hanke, Phys. Rev. Lett. **68**, 1359 (1992).
[18] J. J. Deisz, A. G. Eguiluz, and W. Hanke, Phys. Rev. Lett. **71**, 2793 (1993).
[19] M. Jonson, Solid State Comunn. **33**, 743 (1980).
[20] B. N. J. Persson and A. Baratoff, Phys. Rev. B **38**, 9616 (1988).
[21] D. B. Tran Thoai and M. Šunjić, Solid State Commun. **77**, 955 (1991).
[22] M. Šunjić and L. Marušić, Phys. Rev. B **44**, 9092 (1991).
[23] M. Šunjić and L. Marušić, Solid State Commun. **84**, 123 (1992).
[24] L. Marušić and M. Šunjić, Solid State Commun. **88**, 781 (1993).
[25] R. Fuchs and K. L. Kliewer, Phys. Rev. **140**, A2076 (1965).
[26] R. Brako, J. Hrnčević, and M. Šunjić, Z. Phys. B **21**, 193 (1975).
[27] M. Šunjić and A. A. Lucas, Phys. Rev. B **3**, 719 (1971).
[28] P. Moon and D. E. Spencer, *Field Theory Handbook* (Springer-Verlag, Berlin, New York, 1971).
[29] A. R. H. Clarke *et al.*, Phys. Rev. Lett. **76**, 1276 (1996).
[30] D. Šestović and M. Šunjić, Solid State Commun. **98**, 375 (1996).
[31] A. A. Lucas, P. H. Cutler, T. E. Feuchtwang, T. T. Song, T. E. Sullivan, Y. Yuk, H. Nguyen, and P. J. Silverman, J. Vac. Sci. Technol. A **6**, 461 (1988).
[32] E. L. Wolf, *Principles of Electron Tunneling Spectroscopy* (Oxford University Press, New York, 1989).
[33] Z. Lenac and M. Šunjić, Nuovo Cimento B **33**, 681 (1976)
[34] A. A. Lucas, E. Kartheuser, and R. G. Badro, Phys. Rev. B **2**, 2488 (1970).
[35] P. M. Morse and H. Feshbach, *Methods of Theoretical Physics* (McGraw-Hill, New York, 1953).
[36] R. Straton, J. Phys. Chem. Solids **23**, 1177 (1962).
[37] K. S. Kölbig, Comput. Phys. Commun. **23**, 51 (1981).